The Ductile-to-Quasi-Brittle Transition of Particulate-Filled Thermoplastic Polyester

J. X. LI,[1] M. SILVERSTEIN,[2] A. HILTNER,[1,*] and E. BAER[1]

[1]Department of Macromolecular Science and Center for Applied Polymer Research, Case Western Reserve University, Cleveland, Ohio 44106; [2]Department of Materials Engineering, Technion Israel Institute of Technology, Haifa 32000, Israel

SYNOPSIS

The effects of various filler characteristics on the ductility of filled amorphous copolyester, Kodar 6763, have been examined. The five fillers in the study included two calcium terephthalates with different particle-size distributions and three calcium carbonates, also with different particle-size distributions. One of the calcium carbonate fillers had received a surface treatment. The increase in Young's modulus with increasing filler content was the same for all fillers and was satisfactorily described by Kerner's equation. The only filler to affect the yield stress was the surface-treated calcium carbonate; in this case, the decrease in yield stress was attributed to cracking and splitting of aggregated particles. A sharp drop in fracture strain was observed with increasing filler content. This ductile-to-quasi-brittle transition occurred when the fracture mode changed from fracture during strain-hardening or neck propagation to fracture during neck formation. The critical filler content of the ductile-to-quasi-brittle transition varied from one filler to another. A simple model qualitatively described the decrease in critical filler content with increasing breadth of the particle-size distribution and, in particular, with increasing volume percent of large particles in the distribution.

INTRODUCTION

Calcium carbonate is frequently used as a filler in polymers to increase stiffness and decrease cost. Particle sizes in the range of 1–50 μm are typical, and the particles usually have a low aspect ratio and a broad size distribution.[1,2] Loss of ductility is a major concern with filled polymers, and it has been observed that even a small number of large particles may reduce the mechanical properties significantly.[3] Good adhesion between particle and matrix is generally considered desirable because it can result in higher values of modulus and strength.[4,5] Since calcium carbonate does not exhibit good adhesion to most polymers, various surface treatments and coupling agents have been used to try to improve this aspect.[6–8]

An alternative strategy involves fillers that are inherently more compatible with polymers. Some metal terephthalates have been found to have exceptionally high decomposition temperatures and unusually low solubilities.[9] These salts can be prepared in the form of fibers with high aspect ratios and also as uniform particles on the micron-size scale. With the organic filler, there is the possibility for achieving good adhesion by specific interactions between filler particle and polymer. This possibility is explored in the present study by blending calcium terephthalate with a thermoplastic polyester. The properties achieved with the organic filler are compared with properties obtained when calcium carbonate is used as the filler.

MATERIALS AND METHODS

The polymer used in this study was an amorphous copolyester with the trade name Kodar 6763

* To whom correspondence should be addressed.

Journal of Applied Polymer Science, Vol. 52, 255–267 (1994)
 CCC 0021-8995/94/020255-13

(PETG) from Eastman Kodak. The two types of fillers were an organic filler, calcium terephthalate (CaT), and an inorganic filler, calcium carbonate ($CaCO_3$); the fillers are listed together with the suppliers in Table I.

Before blending, the PETG was dried in a vacuum oven for 24 h at 60°C and the fillers were dried in vacuum for the same time but at 100°C. The polymer and the filler were blended in a Brabender mixer at 200°C for 10 min. The dried polymer without filler was subjected to the same mixing conditions in the Brabender and served as the control. Blends with 5, 15, 30, and 50 wt % filler were prepared. These compositions corresponded to 4.5, 13.5, 27, and 45 vol % for CaT and 2.4, 7.0, 14, and 24 vol % for $CaCO_3$.

Particle-size distribution was determined by dispersing the filler particles on the SEM stage, coating them with 90 Å of gold, and measuring the size of more than 400 particles from the micrographs. The particle size after blending was determined by dissolving the PETG matrix with phenol-chloroform, collecting the particles, and examining them in the JEOL JSM-840A scanning electron microscope (SEM).

The filled polymers were compression-molded into 2 mm-thick plaques in a press at 200°C and 450 psi for 5 min, followed by water cooling in the mold. Before compression molding, all samples were dried in vacuum for 12 h at 60°C. To measure the tensile properties, dog-bone specimens were cut to the ASTM D1708 geometry and tested in an Instron testing machine at a crosshead speed of 2 mm/min, which corresponded to a strain rate of 9%/min. Electronic strain gauges were attached for the modulus measurement. Four specimens were tested for each composition and average values of the tensile properties are reported. The necking process was photographed during tensile testing.

The necked region was subsequently fractured in liquid nitrogen parallel to the draw direction in order to reveal the internal morphology. The cryogenic fracture surfaces were coated with 90 Å of gold and examined in the SEM.

RESULTS AND DISCUSSION

Fillers

The calcium terephthalate (CaT) particles as-received were rod-shaped with an aspect ratio of 1–30 and a length up to 35 μm [Fig. 1(a)]. It was found that these particles were broken down into smaller sizes during the compounding with PETG. When the CaT particles (CaT-2) were collected and examined after the PETG matrix was dissolved with phenol-chloroform, the aspect ratio had decreased to 1–9 and the maximum length had decreased to 16 μm [Fig. 1(b)]. In another preparation (CaT-1), the CaT particles were reduced in size in a jet attrition mill before compounding with the PETG. Milling reduced the aspect ratio to 1–8 and the length to a maximum of 8 μm [Fig. 1(c)]. There was no further change in the particle size during processing with PETG.

Two of the calcium carbonate fillers were cubic-shaped particles that differed in terms of the particle

Table I Characteristics of the Fillers

Filler	Description	Particle Size (μm) Range	Average	Manufacturer
CaT	As-received	d = 0.5–15	1.9	Synthetic Products Co., Cleveland, OH
		l = 0.5–35	6.3	Synthetic Products Co., Cleveland, OH
CaT-2	CaT after mixing	d = 0.5–10	2.0	Synthetic Products Co., Cleveland, OH
		l = 0.5–16	4.2	Synthetic Products Co., Cleveland, OH
CaT-1	CaT milled	d = 0.5–4	1.5	Synthetic Products Co., Cleveland, OH
		l = 0.5–8	2.1	Synthetic Products Co., Cleveland, OH
$CaCO_3$-1	Camel-WITE®	0.5–13	2.2	Genstar Stone Products Co., Hunt Valley, MD
$CaCO_3$-2	Camel-CARB®	0.5–33	4.1	Genstar Stone Products Co., Hunt Valley, MD
$CaCO_3$-3	Hakuenka CC	0.5–37	6.1	Shiraishi Kogyo Kaisha Ltd., Hyogo, Japan

d = diameter; l = length.

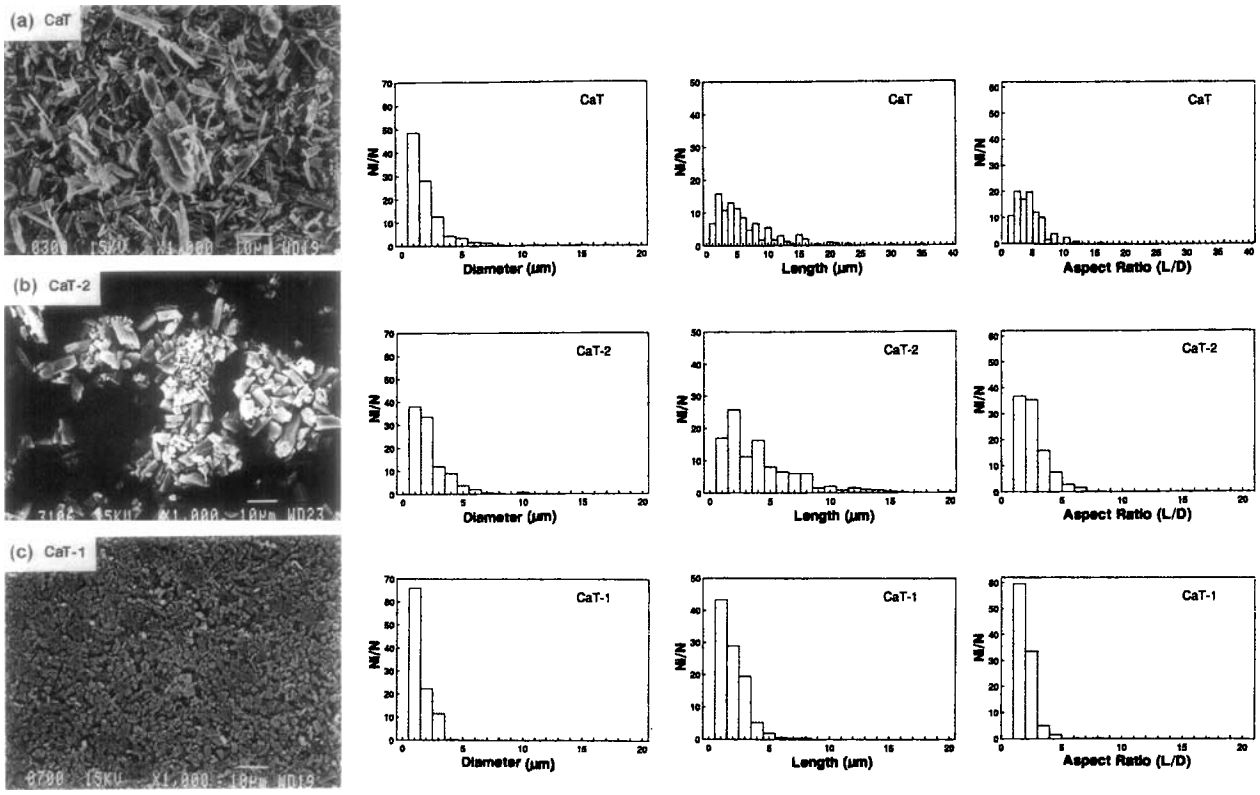

Figure 1 Particle-size distributions for CaT fillers: (a) CaT as received; (b) CaT after compounding with PETG, identified as CaT-2; (c) CaT after milling, identified as CaT-1.

size and particle-size distribution. The average particle size of $CaCO_3$-1 was about 2 μm and the particle-size distribution was fairly narrow with no particles larger than 13 μm [Fig. 2(a)]. The average particle size of $CaCO_3$-2 was 4 μm and the broad size distribution contained some particles as large as 33 μm [Fig. 2(b)]. The $CaCO_3$-3 particles were coated with a fatty acid to promote dispersion during processing. The coating was apparent in micrographs of the particles that had an average size of 6 μm. Aggregation of small particles into larger ones created the broad size distribution [Fig. 2(c)]. The aggregates did not break up during processing.

Stress–Strain Behavior

The stress–strain behavior of unfilled PETG was typical of a ductile polymer. After reaching the yield point, two intersecting shearbands formed across the width of the specimen as the stress dropped to the lower yield stress or draw stress. Local thinning developed from the shearbands with stress-whitening of the thinned region. Subsequently, the neck propagated with a constant stress through the entire gauge section. A region of strain-hardening followed where the stress gradually increased as the necked material extended uniformly until it fractured. Typical engineering stress–strain curves are shown in Figure 3 for PETG filled with CaT-1 and in Figure 4 for PETG filled with $CaCO_3$-2. In general, the yield stress remained constant while the yield strain gradually decreased and the modulus increased with increasing filler content. The feature of the stress–strain curve most strongly affected by the filler was the fracture strain that decreased as the filler content increased.

The increase in Young's modulus of filled PETG with increasing filler content was the same for all the fillers (Fig. 5). The dependence of modulus on filler content was satisfactorily described by Kerner's equation assuming good adhesion between the polymer and the rigid, spherical particle[10–12]:

$$\frac{E_c}{E_m} = 1 + \frac{15(1 - \nu_m)V_f}{(8 - 10\nu_m)V_m} \quad (1)$$

where E_c and E_m are the moduli of filled and unfilled PETG; V_f and V_m, the volume fractions of filler and PETG; and ν_m, Poisson's ratio of PETG ($\nu_m = 0.35$).

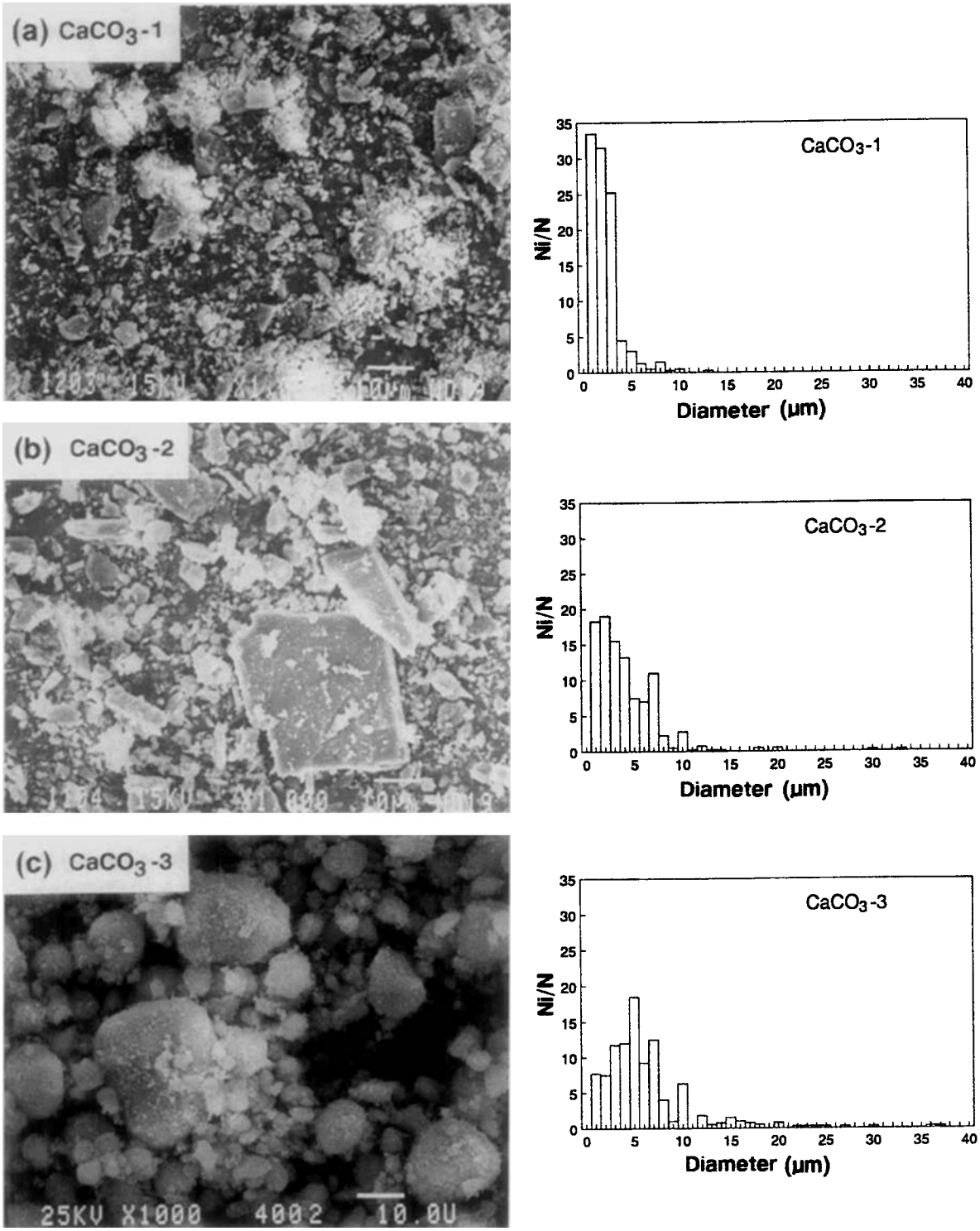

Figure 2 Particle-size distributions for $CaCO_3$ fillers: (a) $CaCO_3$-1; (b) $CaCO_3$-2; (c) $CaCO_3$-3.

The dependence of modulus on filler volume fraction calculated from eq. (1) is included in Figure 5 to demonstrate the good agreement between prediction and experiment.

The yield stress of filled PETG was the same as the yield stress of unfilled PETG; this is generally the case when there is good adhesion between the polymer and the rigid filler.[4,13–15] The yield stress

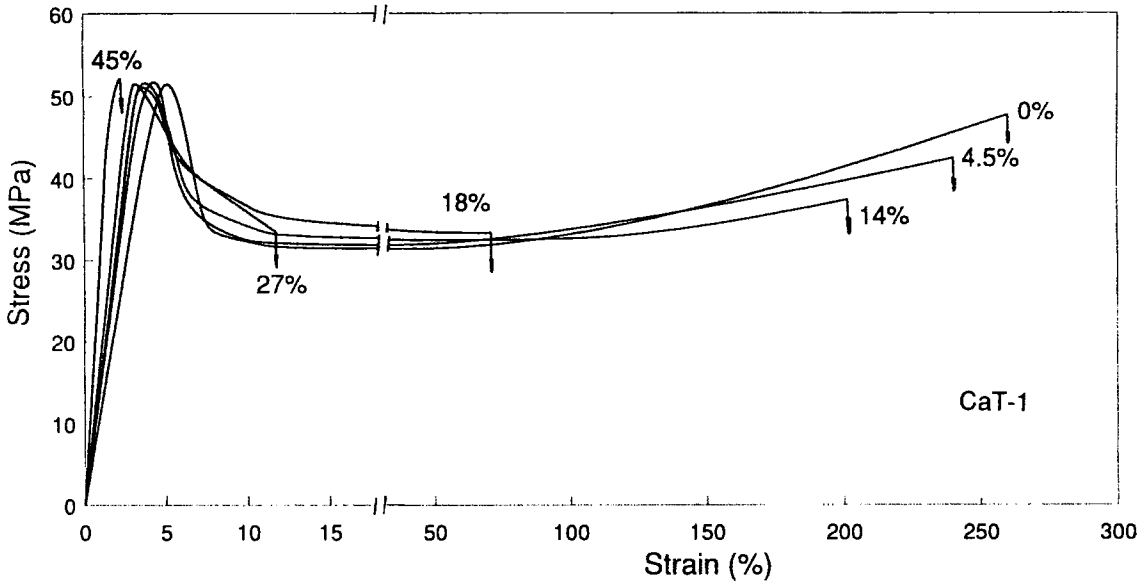

Figure 3 Engineering stress–strain curves of PETG with CaT-1. The filler volume percent is indicated.

did not vary with filler content up to 30 wt % filler or with filler type except for $CaCO_3$-3 (Fig. 6). In this one instance, the yield stress decreased with increasing filler content, which is often indicative of poor adhesion between polymer and filler.[3,16,17] The dependence of yield stress on filler content for the case of debonded particles that are not load-bearing is described by Nielsen's equation[18]:

$$\sigma_{yc}/\sigma_y = (1 - V_f^{2/3}) \qquad (2)$$

where σ_{yc} and σ_y are the yield stresses of filled and unfilled PETG, respectively. Comparison with the data in Figure 6 shows that eq. (2) satisfactorily described the decreasing yield stress of $CaCO_3$-3.

Examination of a fracture surface of PETG with 14 vol % $CaCO_3$-3 showed that debonding of the filler particle from PETG was not the cause of the decreasing yield stress. Instead, internal cracking and splitting of the aggregate particles of $CaCO_3$-3 was observed (Fig. 7). Apparently, before the yield

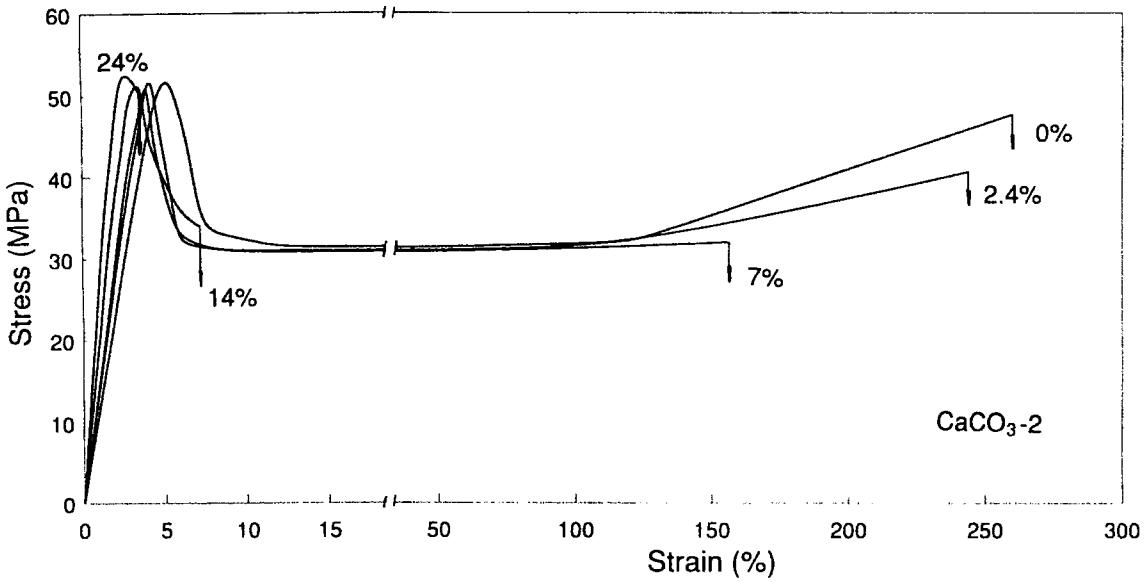

Figure 4 Engineering stress–strain curves of PETG with $CaCO_3$-2. The filler volume percent is indicated.

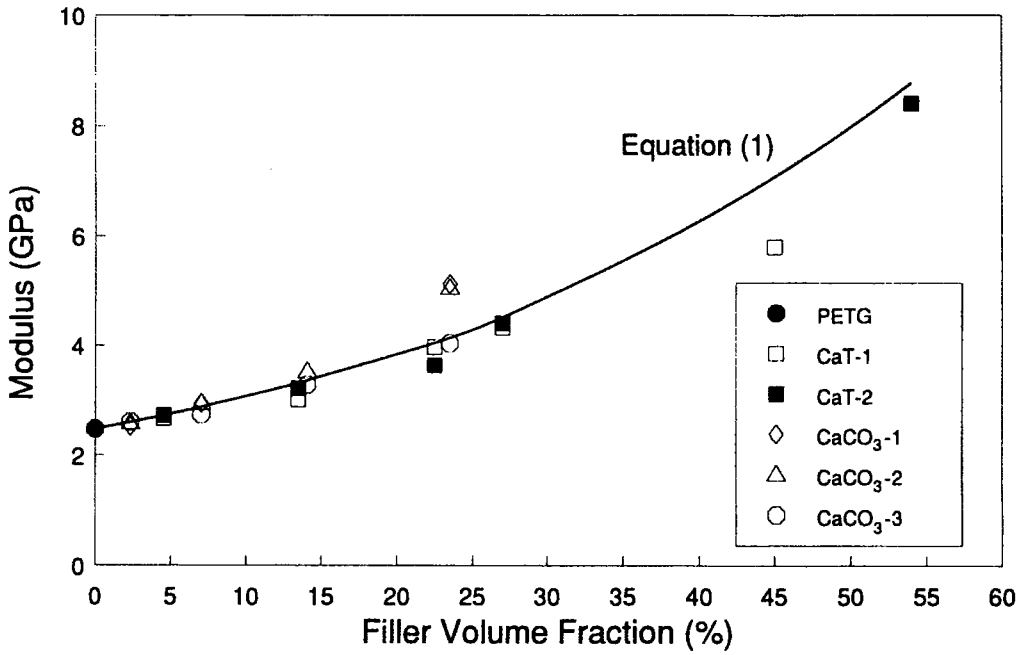

Figure 5 Dependence of the modulus on filler volume percent. The solid curve was calculated from eq. (1).

stress was achieved, the stresses on the aggregate particles were sufficient to cause them to crack. This created a situation, similar to that of debonded particles, where the particles were no longer load-bearing. Consequently, the yield stress was describable by an approach such as Nielsen's that considers only the contribution of the matrix.

The decrease in the engineering fracture stress

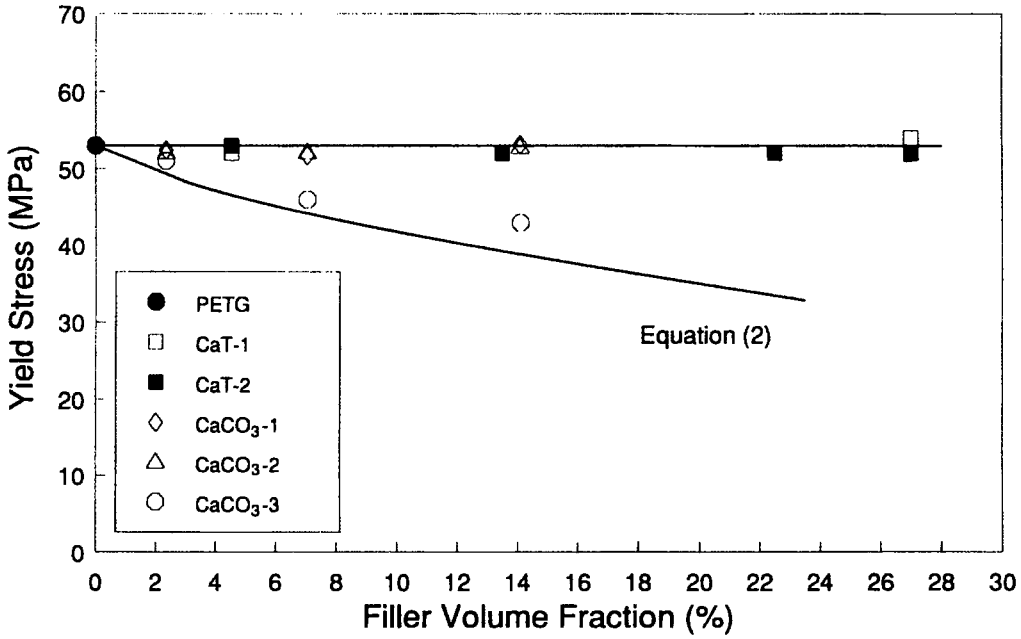

Figure 6 Dependence of the yield stress of filler volume percent. The solid curve was calculated from eq. (2).

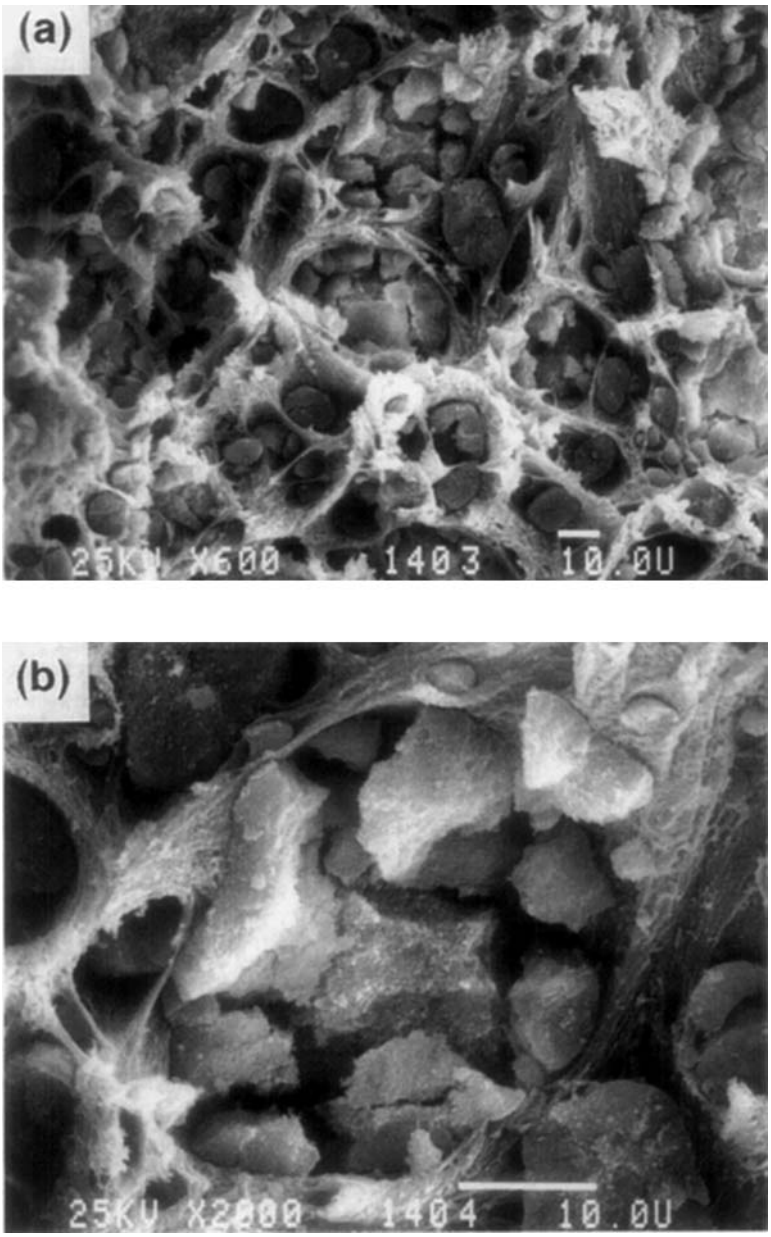

Figure 7 The fracture surface of PETG with 14 vol % $CaCO_3$-3 as viewed in the scanning electron microscope: (a) low magnification showing cracking and splitting of the aggregate particles; (b) higher magnification of one of the split particles.

at lower filler contents reflected the gradual decrease in the strain-hardening region until fracture occurred at a stress equal to the draw stress of PETG. A minimum in the engineering fracture stress was observed at intermediate fillers contents and was equal to the draw stress of PETG. The increase in fracture stress at higher filler contents occurred as a result of fracture during neck formation or just prior to neck formation.

Five fracture modes were observed: As shown schematically in Figure 8, the most ductile compositions fractured during strain-hardening (Mode A) or during neck propagation (Mode B). As the filler content increased, quasi-brittle fracture occurred during neck formation while the stress dropped from the upper yield stress to the draw stress (Modes C and D). Mode C fracture occurred through the thinned region at the site of incipient neck formation

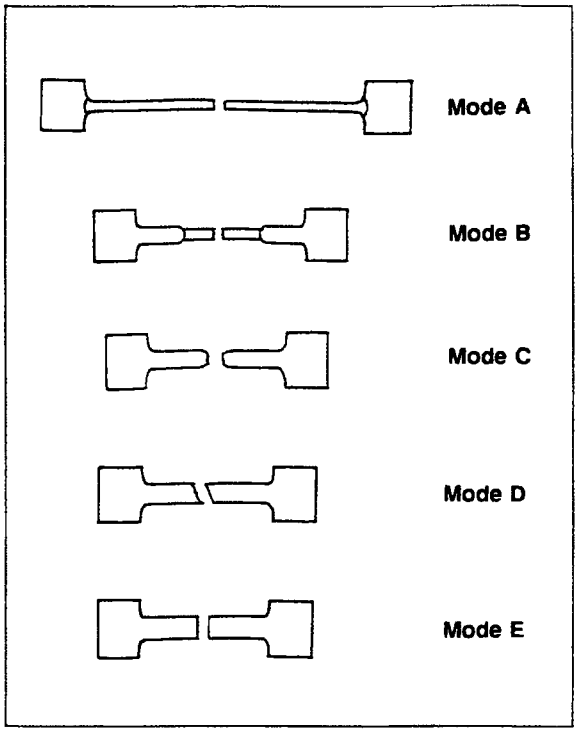

Figure 8 Schematic representation of the five tensile fracture modes.

when the stress had dropped almost to the draw stress. In Mode D, specimens fractured shortly after the yield maximum on the stress–strain curve and fracture occurred through the macro-shearband that formed across the specimen in the beginning of the necking process. In Mode E, specimens fractured in a brittle manner perpendicular to the loading direction before reaching the yield point.

The fracture mode gradually changed from ductile Mode A to brittle Mode E as the filler content increased. However, the fracture mode also depended on the filler, as shown in Figure 9. The influence of filler type was apparent when the effect of 14 vol % on the fracture mode was examined: PETG filled with CaT-1 fractured in the strain-hardening region by Mode A; with CaT-2 and $CaCO_3$-1, fracture occurred during neck propagation by Mode B; and with $CaCO_3$-2 and $CaCO_3$-3, fracture happened during neck formation by Modes C and D, respectively.

Ductile-to-Quasi-brittle Transition

The engineering strain at fracture is plotted as a function of the vol % filler in Figure 10. As the filler content increased, the fracture strain initially decreased only slightly, then decreased sharply at a composition that depended on the filler. This transitional behavior correlated with changes in fracture mode as the filler content increased. The transition corresponded to the change from Modes A and B, when specimens fractured during strain-hardening or neck propagation, to Modes C and D, when fracture occurred during neck formation. A ductile-to-quasi-brittle transition was always observed with increasing filler content. However, the filler content required to achieve the transition varied from one filler to another.

The transition from propagation of a stable neck through the entire gauge length to fracture in the neck without propagation has been described and modeled previously.[19] The model requires debonding during neck formation in order for the matrix polymer to undergo the large local strain required in the necking process. In all the filled polymers, profuse stress-whitening accompanied formation and propagation of the neck. To observe the voids, the necked region was cryogenically fractured parallel to the draw direction. The micrograph of PETG filled with $CaCO_3$-2 in Figure 11(a) shows numerous elongated voids that contain filler particles. The voids have the shape that would be expected if the polymer debonded and drew out around the particles. The micrograph in Figure 11(b) shows similar elongated voids in PETG filled with $CaCO_3$-3. In the largest void seen in the micrograph, a large aggregated $CaCO_3$-3 particle broke up into smaller particles. Slightly above, some smaller elongated holes that formed when the PETG drew out around small nonaggregated $CaCO_3$-3 particles are visible.

The model uses a microscopic failure condition to predict macroscopic mechanical behavior. The condition for quasi-brittle fracture is obtained at a critical filler volume fraction when the local stress

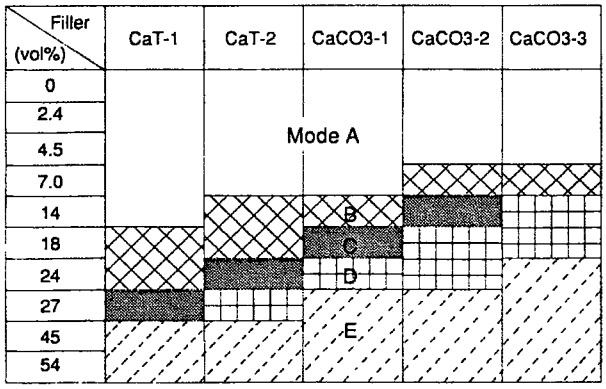

Figure 9 Map of the fracture modes for the various fillers as a function of filler volume percent.

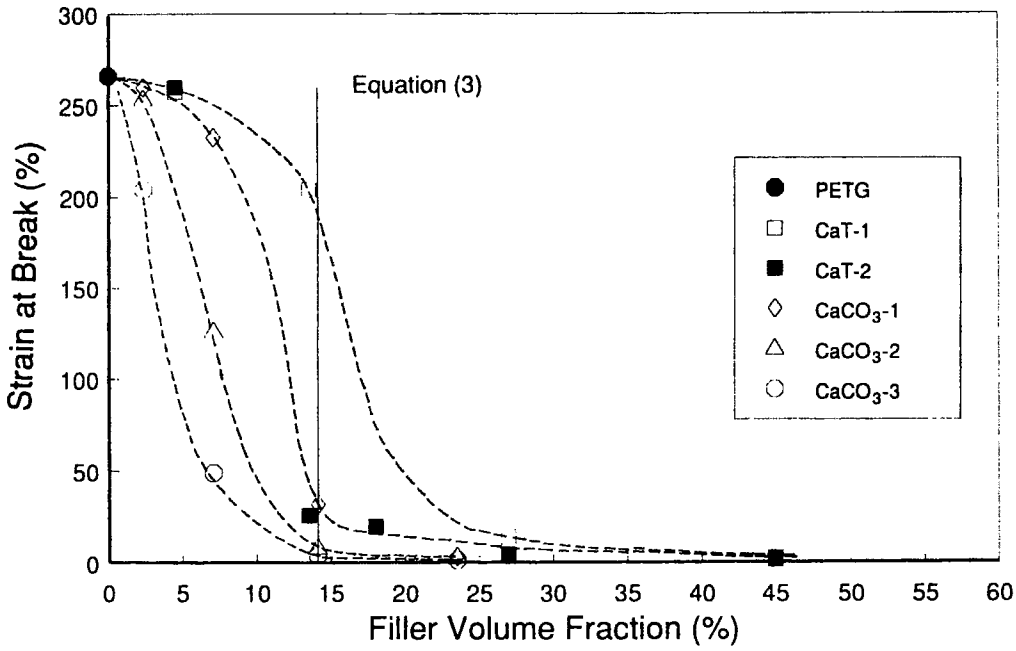

Figure 10 Fracture strain of PETG as a function of filler volume percent showing the ductile-to-quasi-brittle transition.

on the ligaments between the debonded filler particles reaches the tensile strength of the polymer and the ligaments can no longer sustain the engineering draw stress. If it is assumed that the particles are spherical of uniform size and arrayed in a cubic lattice, the critical filler volume fraction is given by

$$V_f^* = [(1/\beta)(1 - \sigma_d/\sigma^*)]^{3/2} \qquad (3)$$

where V_f^* is the critical filler volume fraction for quasi-brittle fracture; σ_d and σ^*, the draw stress and tensile strength of the matrix, respectively; and β, a geometric parameter that for spherical particles is equal to 1.209. Using values of σ_d = 32.6 MPa and σ^* = 48.0 MPa for PETG, eq. (3) predicts a critical filler content of about 14 vol %. This compares to the observed values that were in the range of 10–20 vol %. For two of the fillers, CaT-2 and $CaCO_3$-1, the critical filler content was close to the predicted value; it was slightly lower than predicted for $CaCO_3$-2 and was significantly lower than predicted for the filler with aggregated particles, $CaCO_3$-3.

The critical filler content was higher than predicted for CaT-1. This filler had the narrowest particle-size distribution and thus most closely met the condition of uniform particle size. The stress–strain curves, particularly for the key transitional compositions of 18 and 27 vol % filler, also revealed a feature that differentiated this filler from the others. In the neck formation region, as the engineering stress dropped from the upper yield stress to the draw stress, the stress drop was more gradual, possibly because the particles were not completely debonded and remained at least partially load-bearing during necking.

Effect of Particle-size Distribution

To obtain eq. (3), it is assumed that the critical filler volume fraction depends only on the strain-hardening characteristics of the polymer and does not depend on the properties of the filler as long as the filler particles can be assumed to be spherical and of uniform size. The particle-size distributions of the five fillers are compared by volume fraction in Figure 12. The condition of uniform particle size was most closely met by CaT-1, where the largest particles were about 4 μm in diameter. The distribution was very similar for CaT-2 and $CaCO_3$-1, and broader than for CaT-1, with the largest particles in the 10–15 μm range. Both $CaCO_3$-2 and $CaCO_3$-3 contained some very large particles in the 30–40 μm range. Although the number of large particles was small, the contribution on a volume basis was significant. For example, the large particles with diameters in the 30–35 μm range constituted about 40% of $CaCO_3$-2 by volume. Although $CaCO_3$-3 had

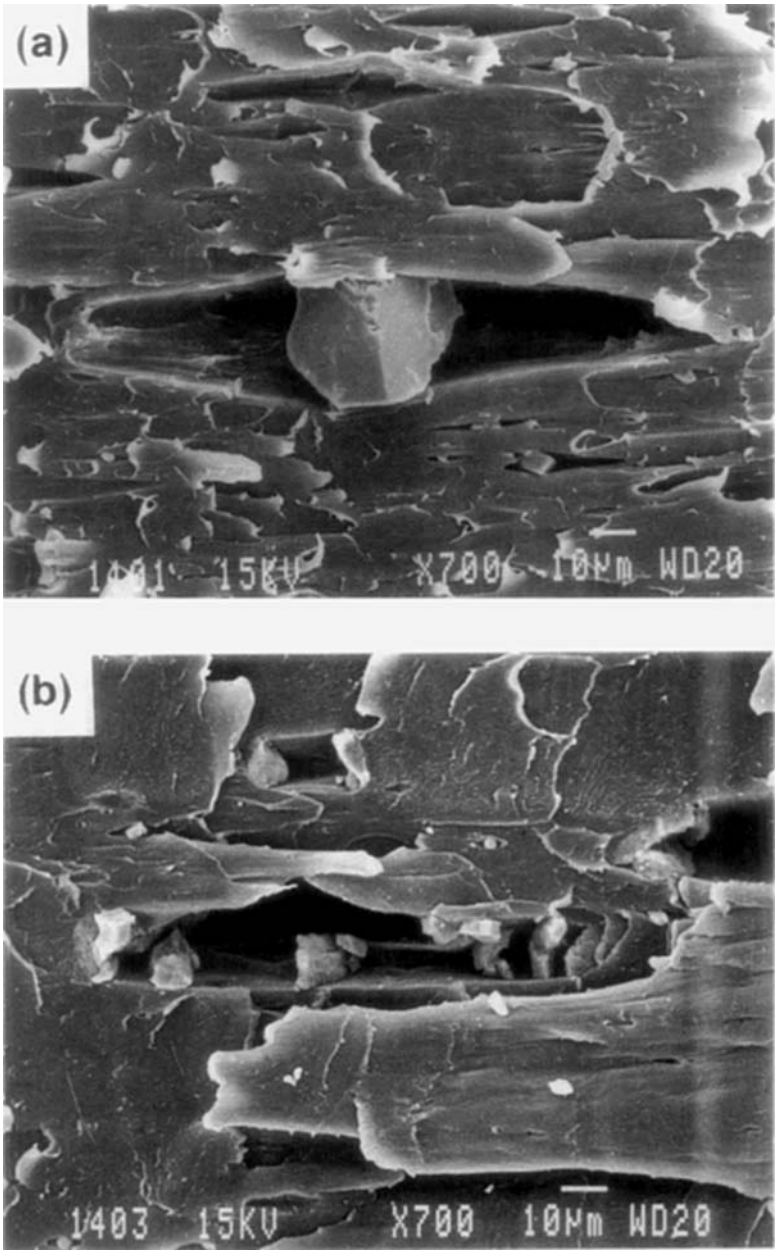

Figure 11 The necked region of tensile specimens that were cryogenically fractured parallel to the draw direction and viewed in the scanning electron microscope: (a) PETG with 2.4 vol % $CaCO_3$-2; (b) PETG with 2.4 vol % $CaCO_3$-3.

an even broader distribution than did $CaCO_3$-2, this filler was not included in the discussion of size-distribution effects because internal cracking and splitting of the aggregate particles produced a different deformation mechanism.

The effect of particle-size dispersion can be easily estimated by assuming that the distribution is bimodal and the difference between the two particle sizes is large. Following the approach used to obtain eq. (3), it is further assumed that the two populations are arrayed in separate, superimposed cubic lattices. The cross-sectional plane that contains the least amount of load-bearing matrix material is the plane that contains the centers of debonded particles of both sizes. If the volume fractions of small and large particles are, respectively, V_{f1} and V_{f2}, the

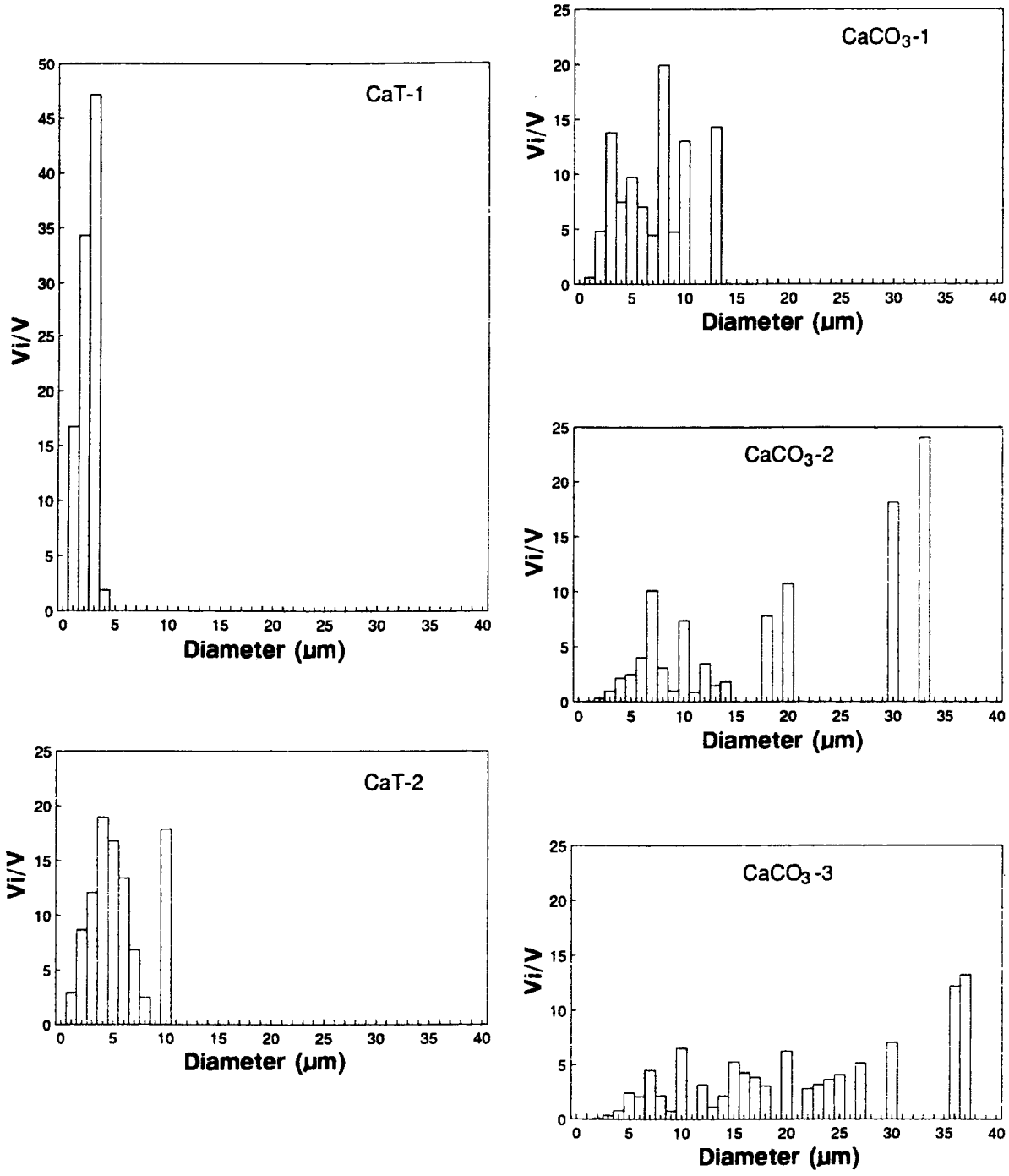

Figure 12 Particle-size distributions on the basis of volume fraction: (a) CaT-1; (b) CaT-2; (c) $CaCO_3$-1; (d) $CaCO_3$-2; (e) $CaCO_3$-3.

critical condition when the strain-hardening strength of the polymer is not sufficient to sustain the engineering draw stress is given by

$$(V_{f1}^{2/3} + V_{f2}^{2/3})^* = (1/\beta)(1 - \sigma_d/\sigma^*) \quad (4)$$

To determine V_f^* for a bimodal distribution [where V_f^* is equal to the sum of the V_{f1} and V_{f2} values that satisfy eq. (4)], it is necessary to express V_{f1} in terms of V_{f2}. The critical filler content is largest when V_{f1} or V_{f2} is zero and eq. (4) reduces to eq.

(3). Increasing the fraction of the second particle size causes the critical filler content to decrease to a minimum when $V_{f1} = V_{f2}$. Only small amounts of the second particle size are required to reduce the critical volume fraction significantly. If the second particle size constitutes 5% of the filler by volume, the critical volume fraction V_f^* for PETG is reduced from 14 to 12%; if the second particle size is 20% of the filler, the critical volume fraction is further reduced to 10%. A further increase in the percent of the second particle size to 50% only changes the critical volume fraction slightly.

The decrease in V_f^* from about 14% for CaT-2 and $CaCO_3$-1 to about 10% for $CaCO_3$-2 was predicted surprisingly well by this approximate model. The particle-size distribution of CaT-2 and $CaCO_3$-1 was approximated by a single particle size and the observed value of 14% for V_f^* was obtained with eq. (3). The much broader distribution of $CaCO_3$-2 was approximated by a combination of two particle sizes. Particles of 20 μm or less that were in the same size range as the particles of $CaCO_3$-1 constituted about 60% of $CaCO_3$-2 by volume, whereas the large particles in the 30–35 μm range constituted about 40% by volume. Using values of 0.6 and 0.4 for V_{f1} and V_{f2} in eq. (4), the calculated critical volume fraction decreased from 14 to 10%.

Draw Strain

Since the engineering draw stress does not depend on the filler content and is the same as the draw stress of the unfilled polymer, the true stress sustained by the polymer ligaments in the neck during neck propagation is higher in cross sections that contain particles than in cross sections that do not. Due to the higher stress, the strain is higher in cross sections that contain particles. This leads to a net increase in the draw strain, i.e., the strain in the necked material while the neck is propagating. The draw strain is predicted for the cubic array of uniform spherical particles as[19]

$$\varepsilon_d = \varepsilon_d^0 + (\sigma_d/E_d)V_f \qquad (5)$$

where ε_d is the draw strain of the filled polymer; ε_d^0, the draw strain of the unfilled polymer; and E_d, the slope of the strain-hardening region of the stress–strain curve.

Two methods were used to estimate the draw strain. In the first, the draw strain was taken from the engineering stress–strain curve as the point where the draw region of constant stress ended and the work-hardening region of gradually increasing stress began. Most of the data points in Figure 13

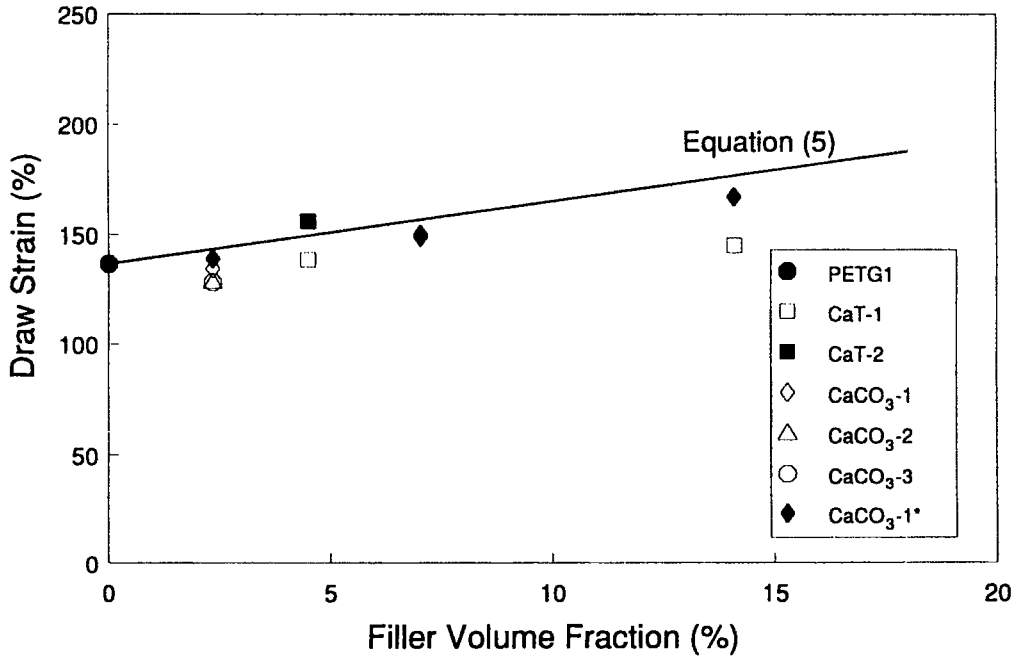

Figure 13 The draw strain of PETG as a function of filler volume percent. The solid line was calculated from eq. (5).

were obtained by this method. Alternatively, the draw strain was measured from the change in separation of marks on the gauge section of the tensile specimens. Figure 13 includes values of the draw strain obtained by both methods for PETG filled with $CaCO_3$-1. Comparison with the curve predicted from eq. (5) shows the gradual increase in draw strain with increasing filler content.

CONCLUSIONS

The influence of various filler characteristics on the ductility of PETG was examined. The five fillers chosen permitted comparisons to be made between an organic filler and an inorganic filler and also revealed the effects of particle size, particle-size distribution, and surface treatment. The observations were compared with predictions made from a simple model. The study led to the following conclusions:

1. The increase in Young's modulus with increasing filler content was the same for all fillers and was satisfactorily described by Kerner's equation.
2. The yield stress was not affected by four of the five fillers. The decrease in yield stress observed with the fifth filler was attributed to breakup of aggregated particles and was described by Nielsen's equation.
3. A ductile-to-quasi-brittle transition characterized by a sharp drop in fracture strain was observed with increasing filler content. The transition occurred when the fracture mode changed from fracture during strain-hardening or neck propagation to fracture during neck formation.
4. The critical filler content of the ductile-to-quasi-brittle transition varied from one filler to another. A simple model was used to estimate the dependence of the critical filler content on particle-size distribution.

The authors thank Dr. Richard Grossman, Synthetic Products Co., for supplying the calcium terephthalate. This research was supported by the Army Research Office (DAAL03-88-K-0097) and the NASA Center for the Commercial Development of Space on Materials for Space Structures.

REFERENCES

1. G. Levita, A. Marchetti, and A. Lazzeri, *Polym. Compos.*, **10**, 39 (1989).
2. H. S. Katz and J. V. Milewski, *Handbook of Fillers for Plastics*, Van Nostrand Reinhold, New York, 1987.
3. S. Ahmed and F. R. Jones, *J. Mater. Sci.*, **25**, 4933 (1990).
4. J. Spanoudakis and R. J. Young, *J. Mater. Sci.*, **19**, 487 (1984).
5. A. C. Moloney, H. H. Kaush, and H. R. Stieger, *J. Mater. Sci.*, **19**, 1125 (1984).
6. Y. N. Sharma, R. D. Patel, I. M. Dhimmar, and I. S. Bhardway, *J. Appl. Polym. Sci.*, **27**, 97 (1982).
7. Q. Fu and G. Wang, *Polym. Eng. Sci.*, **32**, 94 (1992).
8. S. Wu, *Polymer Interface and Adhesion*, Marcel Dekker, New York, 1982, p. 279.
9. P. Baker and R. F. Grossman, *J. Vinyl Technol.*, **11**, 59 (1989).
10. L. E. Nielsen, *Mechanical Properties of Polymers and Composites*, Marcel Dekker, New York, 1974, Vol. 2, p. 382.
11. R. M. Christensen and K. H. Lo, *J. Mech. Phys. Solids*, **27**, 315 (1979).
12. E. H. Kerner, *Proc. Phys. Sci.*, **69B**, 808 (1956).
13. L. Nicholais and L. Nicodemo, *Polym. Eng. Sci.*, **13**, 469 (1973).
14. S. Sahu and L. J. Broutman, *Polym. Eng. Sci.*, **12**, 91 (1972).
15. A. S. Kenyon and H. J. Duffy, *Polym. Eng. Sci.*, **7**, 189 (1967).
16. L. Nicolais and M. Narkis, *Polym. Eng. Sci.*, **11**, 194 (1971).
17. G. Levita and A. Marchetti, *Polym. Compos.*, **10**, 39 (1989).
18. L. E. Nielsen, *J. Appl. Polym. Sci.*, **10**, 97 (1966).
19. S. Bazhenov, J. X. Li, A. Hiltner, and E. Baer, *J. Appl. Polym. Sci.*, **52**, 243 (1994).

Received October 23, 1992
Accepted January 5, 1993